R. J. von Gutfeld
R. E. Acosta
L. T. Romankiw

Laser-Enhanced Plating and Etching: Mechanisms and Applications

We have developed experimental electroplating, electrodeless plating, and etching techniques that use a focused laser beam to define the localized plating or etching region. Enhancements in plating (etching) rates up to $\approx 10^3$ to 10^4, compared to background rates, have been observed in the region of laser irradiation. A thermal model has been developed to describe the observed effects over the entire overpotential (polarization) curve. In the low overpotential region the enhancement is dominated by the increase in the local charge-transfer kinetics due to the local increase in temperature produced by absorption of the laser energy by the cathode (anode). At higher overpotentials, in the mass-transport-limited region, the main enhancement occurs due to hydrodynamic stirring caused by the the large local temperature gradients. Examples of gold, nickel, and copper electroplating are described to illustrate the value of this technique for micron-sized circuit personalization and repair. Additional examples of electroless laser-enhanced plating and exchange plating are also described.

Introduction

Recently, an interesting and novel application of lasers was discovered in which a laser beam impinging on an electrode is used to enhance local electroplating or etching rates by several orders of magnitude [1, 2]. It has also been discovered that with the aid of the laser it is possible to produce very highly localized electroless plating at high deposition rates, to greatly enhance and localize the typical metal-exchange (immersion) plating reactions, to obtain thermo-battery-driven reactions with simple single-element aqueous solutions, and to greatly enhance localized chemical etching. Since laser beams can be readily focused to micron-sized dimensions and scanned over sizeable areas, the enhancement scheme makes it possible to plate and etch arbitrary patterns without the use of masks. After a brief summary of the early results, we review the recent experiments designed to help us understand and further explore the observed laser plating and etching enhancement phenomena. Some examples of laser-enhanced plating requiring no external power sources are also described. Applications of these new techniques, particularly to maskless microcircuit repair and design changes, are discussed.

Laser-enhanced electroplating and etching

• *Two-electrode system*

The first results in laser-enhanced plating and etching, using a simple two-electrode system, were described by von Gutfeld *et al.* [2]. A small glass cell containing the two electrodes separated by ≈ 1 cm and containing one of several electrolytes was positioned in front of a focused argon or krypton laser beam. The anode was generally platinum (considered electrochemically inactive), while the cathodes consisted of thin glass slides containing evaporated films of one of several metals, such as Ni, Mo, Cu, or W ($\approx$20–200 nm). The evaporated films served the dual purpose of making the glass electrically conductive and optically absorbing. A schematic of the experimental arrangement is shown in Fig. 1(a). Laser-enhanced plating (or etching) was observed when a small (1.6–2.2 V) dc potential was applied between the cathode and anode, with the laser directed onto the cathode either at the electrolyte–thin-film or glass–thin-film interface (through the glass). As shown in the figure, the laser could be operated in a pulsed or continuous-

wave (cw) mode. The plating solutions were standard acid-copper and dilute nickel chloride electrolytes; see Table 1. Electro-etching of stainless steel was carried out using a dilute nickel chloride electrolyte. The applied plating (etching) voltage was also either applied continuously or pulsed synchronously with the laser so that the voltage and laser pulses overlapped. These combinations of different parameters have now been successfully demonstrated for both plating and etching, although their optimization has not been extensively explored. For most of the early plating and etching work, a cw voltage of ≈2 V, in combination with a pulsed laser beam of ≈1–40-ms duration, was used. The plating/etching current was monitored across a dropping resistor and measured on an oscilloscope. To obtain micron-sized patterns, a separate cell [see Fig. 1(b)] was designed to fit onto a microscope stage. In this manner we were able to utilize the convenience of a microscope both to focus the laser and to view the resulting pattern. Some examples of plating and etching using a nickel chloride electrolyte are shown in Fig. 2. Figure 2(a) shows plated Ni spots ≈4 μm in diameter and 50 nm thick, which have been deposited onto a W film predeposited onto glass. These spots were obtained by continuously moving the microscope stage while shining 0.3-ms pulses of argon laser light onto the cathode. The Ni-plated lines in Fig. 2(b) were made using a cw laser directed onto the cathode while slowly but continuously moving the microscope stage. Figure 2(c) shows an electro-etched hole produced with a pulsed argon laser. Here, the anode and cathode were interchanged from the arrangement used in Fig. 1(b) by reversing the polarity of the applied voltage. The resulting etched hole, 25 μm in diameter, was produced in a 50-μm-thick stainless steel foil that was used as the anode. No post-laser-etch processing was used to obtain the circumferential uniformity or verticality of the hole. The nickel electro-etching solution used had the composition shown in Table 1.

We have plated Ni, Cu, and Au spots and lines and have etched holes and slots in a variety of thin films on glass and thin foil materials using both configurations shown in Fig. 1. Electroplating and electro-etching rates as high as 10 μm/s have been observed using laser power densities of $\approx 10^5$ W/cm^2. In general, enhancement of plating (etching) is observed for power densities of 10^2 to 10^6 W/cm^2 for cathodes (anodes) having an optical reflection coefficient on the order of 0.50. Higher reflectivities require higher incident laser power densities to obtain similar enhancements. All of our experiments used standard Ar or Kr lasers with maximum available power outputs of ≈0.5 W. The optical wavelength for any particular experiment was chosen such that absorption by the electrolyte would be minimized. Thus, the Ar laser (514.5 nm) was used for Ni (green) or Cu (blue) plating solutions, while the Kr laser (647.1 nm) was used for plating Au from the gold–cyanide solution (light yellow).

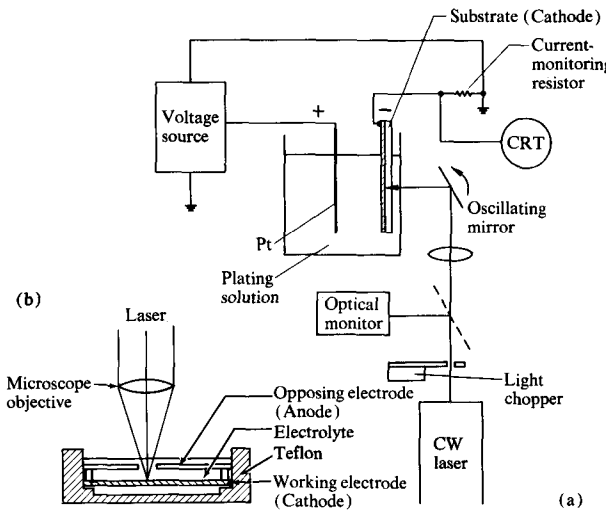

Figure 1 (a) Experimental arrangement for studying laser-enhanced plating and etching, shown here with backwall illumination. (b) A cell used in conjunction with an optical microscope for fabricating small plating and etching patterns.

Table 1 Electrolyte solutions for nickel electroplating and electro-etching and copper electroplating and metal exchange. Weights and volumes given are for one liter of solution.

Ni	*Cu*
$NiCl_2 \cdot 6H_2O$, 27.25 g H_3BO_3, 6.25 g Na saccharin, 0.2 g Na lauryl sulfate, 0.2 g pH (HCl), 2.5	$CuSO_4 \cdot 5H_2O$, 225 g (0.9 M) H_2SO_4 (conc.), 50 ml HCl (10%), 0.3 ml
	$CuSO_4 \cdot 5H_2O$, 50 g (0.2 M) H_2SO_4 (conc.), 25 ml *HCl (10%), 0.3 ml* Thiourea*
	$CuSO_4 \cdot 5H_2O$, 12.5 g (0.05 M) H_2SO_4 (conc.), 36 ml

*Levelers M & T Co., grain refiner's thiourea.

Plating and etching enhancement rates were determined by two independent methods. The first consisted of comparing the plating (etching) current across the monitor resistor (see Fig. 1) with and without application of the laser. To obtain the enhancement factor (ratio) from these measurements required normalization to equal areas since the laser-irradiated area is much smaller than the total cathode (anode) area. Thus, it is the ratio of the current densities that defines the enhancement, and this ratio was found to be in good agreement with the ratios of film thicknesses obtained for the laser-exposed and unexposed areas using a Talysurf 4 (Taylor and Hobson) step profiler. The enhancement in plating current is shown as a function of light

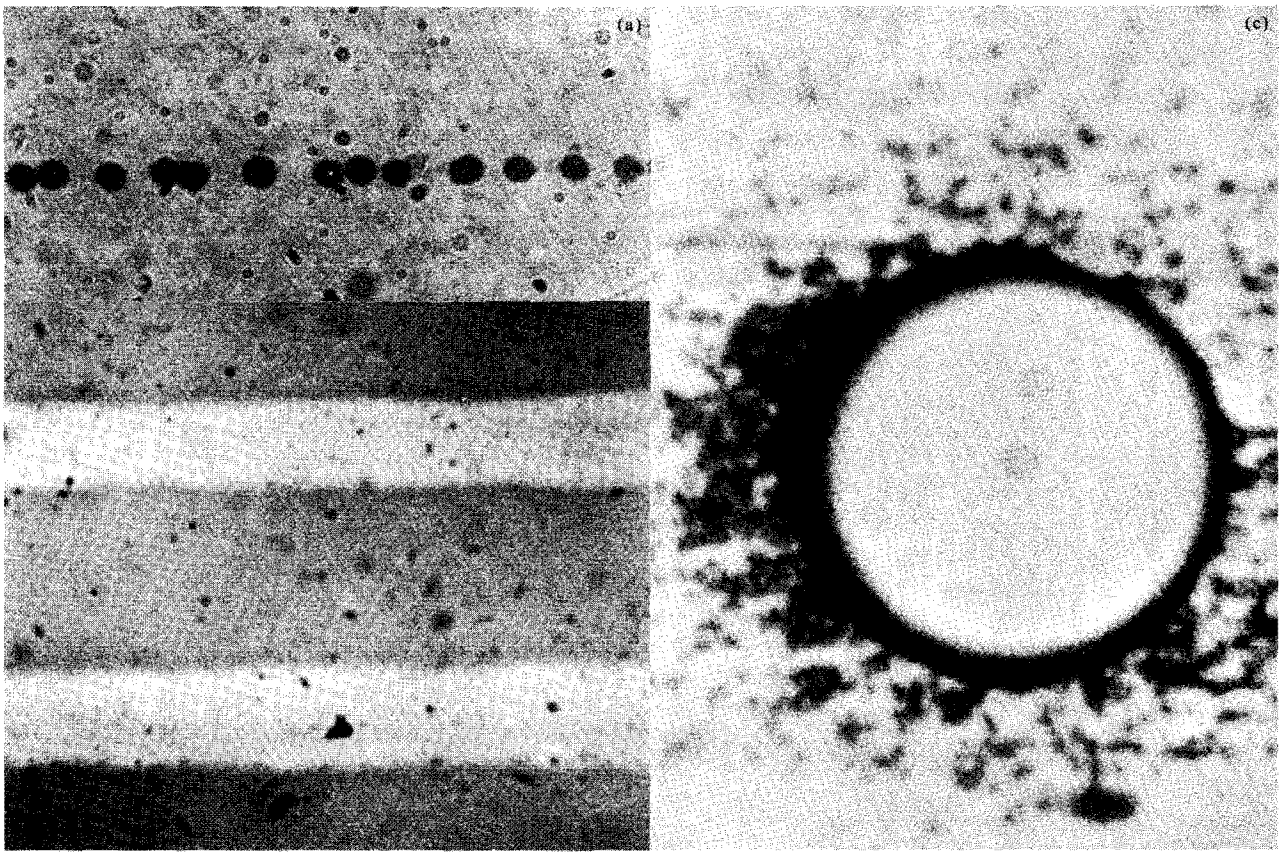

Figure 2 (a) Nickel spots ≈50 nm thick and 4 μm in diameter made with 0.3-ms pulses. (b) Ni stripes ≈200 nm thick and 20 μm wide made with cw laser. Tungsten, 200 nm thick, was predeposited on glass to serve as electrodes in both cases. (c) 50-μm laser-etched hole in 50-μm-thick stainless steel shim stock.

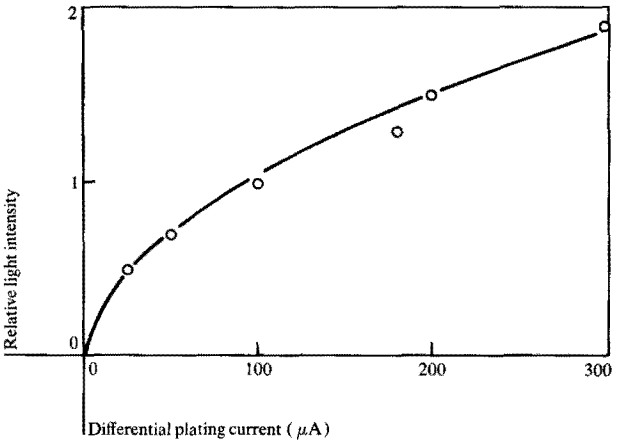

Figure 3 Plot of the relative enhancement current with relative light intensity measured across the dropping resistor of the set-up in Fig. 1.

intensity in Fig. 3 for a cathode–anode voltage of ≈2 V. The values for the current and current density were obtained by measuring the peak ac voltage appearing across the monitor resistor upon application of pulsed laser light to the cathode. While initially quite nonlinear, the enhancement current increases with increasing laser power and becomes linear at the higher laser power densities used.

The early explanation for the observed enhancement ratio for electroplating was based mainly on the assumption that localized thermal convection ("microstirring") in the electrolyte resulted in thinning of the diffusion layer. This local thinning would give rise to spherical diffusion and current crowding into the irradiated region, which would in turn greatly enhance the electroplating rate [1, 2]. In the case of electroless and immersion plating, the observed enhancement was attributed to a local change in the free energy of reaction F^0, such as that typically observed in electroless and metal-exchange (immersion) plating when the temperature of the solution is raised from room temperature to a common operating temperature of 60–90°C.

A number of experiments were performed to prove that the observed enhancement mechanism is principally a ther-

mal rather than photolytic or photon-assisted effect. In one experiment we used two dielectric cathode substrates with widely differing thermal conductivities, glass and single-crystal sapphire. Each had a thin evaporated film of W (≈200 nm) to form the required electrically conductive layer for the cathode. With equal laser power densities incident at the electrolyte–W film interface we found an order-of-magnitude-smaller plating thickness for the sapphire substrate compared to the glass; the plated spot diameter was also considerably larger for the sapphire. We interpret these results in terms of the increased thermal spread and the lower final temperature attained by the sapphire compared to the glass electrode. In a related experiment, we compared the plating thickness attained with frontwall (through the electrolyte–metal-film interface) and backwall (through the glass–metal-film interface) illumination of the cathode surface. Both the spot diameter and plating thickness were approximately equal for the two cases. For backwall illumination, photons cannot reach the electrolyte once the plating thickness is greater than ≈200 nm; however, the thermal energy can readily spread to the film–electrolyte interface. Thus, the final temperature at the electrolyte–film interface is nearly the same for these two methods of illumination, allowing for a thermal rather than a photolytic effect.

Plating mechanisms and a thermal model

The early experiments just described in connection with electroplating gave rise to a simple model of microstirring in which the enhancement in plating rates is attributed mainly to a superior supply of the reactive ions at the interface. This model assumes that typical electroplating reactions are diffusion-controlled, with discharge reaction rates that are fast enough for mass transfer to be the rate-limiting step. However, at low overpotentials (not mass-transfer-limited) the copper deposition reaction is well described by the Butler-Volmer equation [3]:

$$i = i_0 \left[\exp\left(\frac{\alpha \eta F}{RT}\right) - \exp\left(\frac{-\beta \eta F}{RT}\right) \right], \tag{1}$$

where i is the current density, i_0 is the exchange current density, η is the overpotential, α and β are exchange coefficients, F is Faraday's constant, and T is the absolute temperature. For an 0.05-molar (0.05-M) $CuSO_4$ solution, the corrected i_0 value is 2.1×10^{-4} A/cm^2. Hence, at room temperature (T = 298 K) and η = 500 mV, the current density expected for this system (assuming an infinite supply of reactant) is i = 3.5 A/cm^2. This current density is well below the current density of 18 A/cm^2 observed by Puippe *et al.* [4] for 0.05-M $CuSO_4$ solutions under laser irradiation. Accordingly, it was of interest to determine how the absorption of laser energy affects the overall process of deposition, *i.e.*, the supply of reactants as well as the reaction itself. In principle, the effect of temperature changes in an electrochemical system can be described in the following manner. The equilibrium of a M/M^{++} system is affected by temperature changes [5];

$$nF\varepsilon^0 = \Delta F^0 \tag{2}$$

and

$$\frac{\partial \Delta F^0}{\partial T} = -\Delta S^0 = \frac{\Delta F^0 - \Delta H^0}{T}. \tag{3}$$

This is the Peltier effect, with n being the number of electrons involved in the electrode reaction, ε^0 the equilibrium potential, F^0 the free energy of the reaction, S^0 the entropy, and H^0 the enthalpy. For a binary electrolyte, the transport equation in the presence of a temperature gradient (no pressure or gravity gradients) becomes [6]

$$\nabla \mu_e + \bar{S}_e \nabla T = \frac{C_0 RT\sigma}{C_0 + C} \nabla T, \tag{4}$$

where σ is the Soret coefficient, μ_e is the electrochemical potential of the electrolyte, $\bar{S}_e$ is the partial molar entropy of the electrolyte, and C_0 and C are the molar concentrations of the solvent and the electrolyte, respectively. The effect of temperature on the kinetics of the reaction may also be taken into account by correcting the Butler-Volmer equation for temperature [3], *i.e.*,

$$i_0 = nF \frac{kT}{h} \exp(-\Delta F^0) \frac{n}{RT} \exp\left(-\frac{\alpha nF}{RT} \varepsilon^0\right), \tag{5}$$

where k is the Boltzmann constant, and h is Planck's constant.

Unfortunately, the phenomena that occur at high temperatures or in nonisothermal electrolytic systems have not been as widely studied as those that occur in isothermal, room-temperature systems, and it is difficult to find published thermodynamic data for use of Eqs. (2)–(5). Hence, to obtain greater detail of the changes that take place under the effects of laser irradiation, a three-electrode system with potentiostatic control was used; see Fig. 4(a) [7]. In this arrangement, a current is passed between the working plating or etching electrode and the counter-electrode in such a way as to maintain a given potential difference between the working electrode and the third reference electrode. The latter is located in close proximity to the former to minimize the (ohmic) potential drop in the electrolyte. With this arrangement it is possible to impose an arbitrary potential on the working electrode without interference from the reactions that occur at the counter-electrode, and thus to study the details of the plating/etching process. The entire *i vs. E* curve (*i.e.*, the polarization behavior) for the Cu/Cu^{++} system in a well-supported electrolyte was studied with and without laser irradiation. To highlight the laser enhancement, a glass sample with a predeposited copper layer was coated with a photoresist layer over its entire surface, except

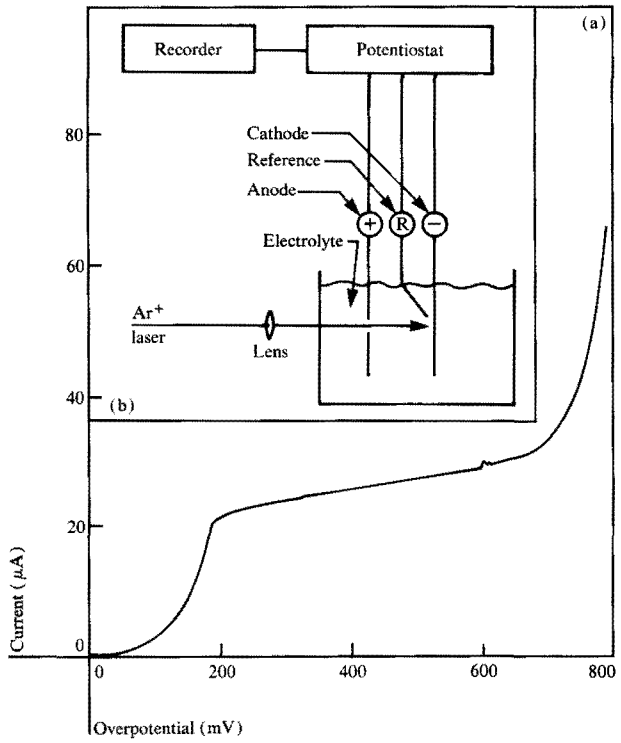

Figure 4 (a) Schematic for laser plating using a three-electrode potentiostatic system. (b) Polarization curve for Cu/Cu^{++} system with a 500-μm-diameter electrode.

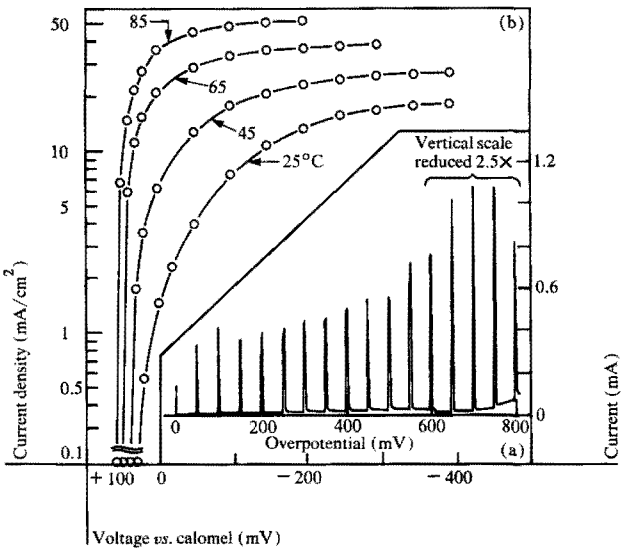

Figure 5 (a) Polarization curve for Cu/Cu^{++} with 200-μm electrode diameter and periodic application of a laser, as indicated by the sharp spikes in the polarization curve. (b) Polarization curves as a function of temperature using a standard rotating-disk technique.

for a small hole with a diameter approximately equal to that of the laser beam. Figure 4(b) shows the resulting polarization curve.

Three distinct regions are in evidence. For low overpotentials the current follows the Butler-Volmer equation. At somewhat higher overpotentials a plateau occurs where the current is quite independent of overpotential. (Beyond this overpotential region the current increases again when another reaction, hydrogen evolution, becomes possible.) This is the mass-transport-controlled region, where the rate of transport of the reactant to the interface is smaller than the rate at which it can be consumed by the charge-transfer reaction. As a result, the concentration of this species approaches zero at the interface. It is important to emphasize that at overpotentials where the limiting current is reached the rate is no longer determined by the potential driving force, and the problem becomes identical to a heat- or mass-transport problem by convective diffusion. As such, the flux of reactant and the reaction rate are now given by equations of the type [6]

$$N_i = Z_i \mu_i F C_i \nabla \Phi - D_i \nabla C_i + v C_i , \tag{6}$$

where N is flux, Z is the charge, μ is the mobility, C is the concentration, Φ is the electric potential, and v is the linear flow velocity. The subscript i refers to the species i.

In the absence of migration flux (in a well-supported electrolyte), the flux at the wall is inversely proportional to the concentration boundary layer thickness δ:

$$N_i = -D_i \frac{\Delta C_i}{\delta} . \tag{7}$$

For a conventional system it is difficult to achieve very thin boundary layers, even with very strong agitation (*i.e.*, $\delta \approx 13$ μm for a rotating disk electrode at 3000 revolutions per minute). The mass-transport-limited reaction rate of 18 A/cm^2 found for the laser-enhanced condition for a 0.05-M $CuSO_4$ solution corresponds to $\delta \approx 0.53$ μm. This seemingly incongruous figure is easier to understand when consideration is given to the very small spot diameter. That is, by definition the boundary-layer thickness is zero at the edge of the mass-transport section, and the "edge" in this case encompasses a large portion of the total mass-transport section. The dominance of this effect in this case is borne out by the inverse dependence of the current density on the spot diameter [4]. The polarization curve for $CuSO_4$ with periodic laser illumination is shown in Fig. 5(a). Here, the laser enhancement is indicated by the sharp spikes in the curve occurring periodically as the voltage is scanned. The electroplating enhancement rates in the mass-transport-limited region are generally consistent with those found in the previously described work. Thus, we believe the very high plating rates and high enhancement ratios reported in the first experiments using a two-electrode system corresponded to the mass-transport-limited region of the polarization curve, as the previous explanation implied.

The potentiostatic experiments clearly point out that enhancement of laser electroplating occurs over the entire polarization curve [4, 7]. At the lower overpotentials, $0 < \eta < 300$ mV (all negative values), application of the laser accelerates the kinetics due to the localized increase in temperature. The increase in reaction rates has been shown in separate studies for the Cu/Cu^{++} system without the use of a laser. Polarization curves as a function of temperature for this system are shown in Fig. 5(b), which indicates that a 60°C increase in temperature for $\eta \approx 50$ mV gives rise to an order-of-magnitude increase in the reaction rate. It is also apparent from these curves that a shift in the equilibrium potential towards a more positive value occurs with increasing temperature. This shift produces an even greater increase in the reaction rate with temperature. The positive shift in the equilibrium potential makes it possible to plate copper at zero overpotential upon application of the laser since the local increase in temperature shifts the current–voltage curve to a more positive potential and to a faster reaction rate curve than that which corresponds to the room temperature condition. In this overpotential regime, local plating occurs with zero background plating, thereby causing the enhancement ratio to approach infinity. At the higher overpotential values ($\eta > 300$ mV), the polarization curve corresponds to the mass-transport-limited regime where microstirring due to thermal convection produces the local plating enhancement. Up to 6 μm/s of plating growth were observed for a plating solution of 0.05 M $CuSO_4$ and 1 M H_2SO_4. This is a very fast plating rate for such a dilute solution. Considerably faster rates can be expected for more concentrated Cu^{++} solutions; however, this remains to be investigated in detail.

Thus, three major factors contribute to the enhancement observed for Cu/Cu^{++}. The equilibrium potential shifts to a more positive value, the kinetics increase with temperature, and microstirring occurs because of locally steep thermal gradients in and around the region of laser absorption. In addition, locally increased temperatures result in an increase of the diffusion rate constant and may result in an increased ionic migration rate and solution conductivity. All of these factors give rise to spherical ionic flux, current crowding, and large potential gradients in the region of the heated spot [2].

An additional enhancement factor in the mass-transport-limited region has recently been shown to result from bubbling in the electrolyte [4]. This situation is achieved by increasing the laser power density at the electrolyte–cathode interface to produce local boiling. Experimentally, these measurements were made using the potentiostatic system shown in Fig. 3, in conjunction with a small audio microphone attached to the side of the plating cell. At the higher power densities, with the aid of a TV monitor, boiling could

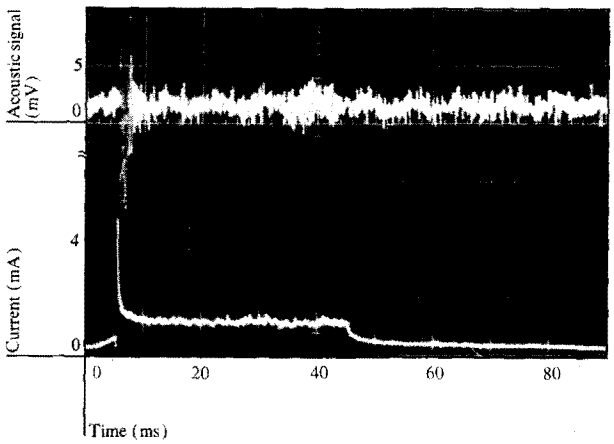

Figure 6 The additional enhancement that occurs with the onset of boiling: Top trace, the acoustic signal; bottom trace, current signal. Boiling is observed at $t = 6$ ms after initiation of the 45-ms laser pulse.

be observed in the form of a stream of bubbles ejected normally from the cathode surface. With 10–20-ms pulses of Ar laser light incident at the electrolyte–Cu film interface, it was possible to correlate the onset of boiling and an additional factor-of-four increase in the plating-enhancement current. These effects were observed by simultaneously monitoring the microphone and the potentiostat current on a dual-beam oscilloscope; see Fig. 6. Upon application of the laser light, the plating current level first increases because of the microstirring. After ≈ 6 ms, an additional increase of approximately a factor of four is observed, occurring at the same time as the onset of acoustic emission due to bubbling detected by the microphone.

Plating without an external power source

A number of laser-enhanced plating effects requiring no external power source have been investigated. The first involves either laser-enhanced electroless Ni plating with sodium hypophosphate as a reducing agent in connection with $PdCl_2$ surface activation, or an electrically activated metallic film surface deposited on glass substrates [2]. Enhanced electroless Ni plating in the region of laser irradiation occurred but at a slower rate than the laser-enhanced Ni electroplating. Almost no background plating was observed. Since no external current flows in these systems, the laser-enhanced growth rates are determined by comparing the thicknesses of unexposed and laser-exposed regions. A plot of the plated thickness as a function of time is shown in Fig. 7. The experimental arrangement consisted of shining a focused cw argon laser beam through a rectangular glass container containing the Ni electroless plating solution and onto the submerged sample.

The lack of significant background plating and the slower plating rates in electroless plating are readily explained in

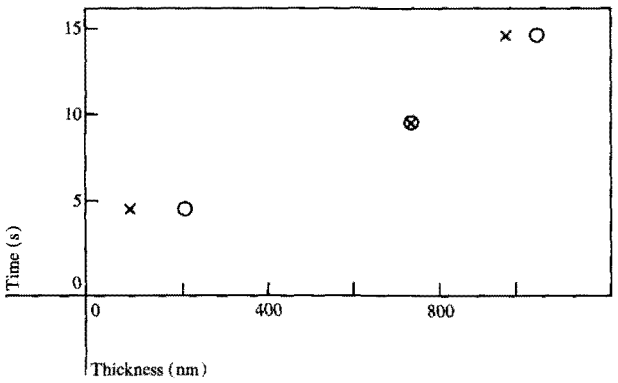

Figure 7 Enhanced electroless nickel plating thickness *vs.* time using frontwall (o) and backwall (×) Ar laser illumination; incident power density was 1 kW/cm^2.

terms of well-known facts. The electroless plating solutions are usually formulated to produce no chemical reaction (no plating) at room temperature and plating at measurable, but controlled, rates at elevated temperatures (≈60–90°C). The plating rate of a typical electroless solution is strongly temperature-dependent, and this temperature dependence closely corresponds to differences in $\Delta F^0_{25°C}$ and $\Delta F^0_{25+\Delta T°C}$, and hence to the shift in the equilibrium constant between 25°C and the plating temperature of $(25 + \Delta T)$°C. The plating rate for the typical well-formulated electroless solution is primarily discharge-controlled, and the mass transport usually does not affect the rate.

Exchange plating will occur under certain conditions when a less noble metal surface is immersed in an electrolyte containing a more noble metal. In general, the process is quite temperature-dependent, with increased exchange plating rates occurring at higher temperatures. This process, like electroless plating, depends primarily on the shift in the equilibrium constant due to differences between $\Delta F^0_{25°C}$ and $\Delta F^0_{25+\Delta T°C}$. In most cases involving well-formulated solutions, the rate is primarily under chemical control. Unlike electroless plating, where the driving force is a reducing agent present in the solution, the driving force here is due to the local differences in the free energy ΔF^0 resulting from the heterogeneous nature of the substrate (*i.e.*, differences in ΔF^0 for intergranular regions and for the surfaces of crystallites). Under normal exchange-plating conditions, the total surface of the metal in an immersion-plating solution becomes covered by a large number of microscopic (grain-size level) anodic and cathodic regions, and the local electrochemical reaction proceeds in each individual microcell until the total surface of the metal is covered with a uniformly thick porous deposit of the more-noble metal.

By heating the surface locally with a laser beam, we have demonstrated that it is possible to establish a $(\Delta F^0_{25°C} - \Delta F^0_{25+\Delta T°C})$ difference greater than $(\Delta F^0_{25°C\ \text{grain}} - (\Delta F^0_{25°C\ \text{intergranular regions}})$. Hence, we have made the part of the surface held at room temperature act as an anode while the laser-illuminated (heated) area acts as a cathode, establishing a thermobattery effect. This effect has been demonstrated by us not only for exchange plating, where the solution contains the more-noble element while the surface being plated consists of the less-noble metal [8], but also for a case where both the metal and element in solution were of the same nobility (Cu substrate immersed in $CuSO_4$) [4]. In this case, the difference in free energy is based strictly on the difference in temperature of two different regions (thermobattery effect). Depending on the direction in which the equilibrium potential shifts, either localized plating or etching occurs. One interesting aspect of laser-enhanced exchange plating is that it should permit plating of a *less-noble* metal onto a more-noble metal surface when the shift in equilibrium potential of the less-noble metal is such that it becomes more positive than the cooler, unexposed more-noble metal. The ability to achieve local thermobattery plating out of a variety of electrolytes on different surfaces and to have dense nearly pore-free deposits opens up several interesting possibilities, including that of completely dispensing with the external field while providing for local electroplating or simultaneous plating and etching.

We have successfully exchange plated Cu (Cu plated out of acidic $CuSO_4$ solutions) on Ni, W, Cr, and Cu; and Au (Au plated out of ®Oromerse exchange plating solution supplied by Technic Corp. of Cranston, RI) on Ni, Cu, and W. In general, the laser-enhanced exchange plating continues until the peripheral electrode region is totally etched, thereby breaking contact between the region being plated and that which maintains overall charge neutrality through etching. This simultaneous plating and etching is rather novel. Patterns that are electrically isolated from the surrounding metallization can be created. Examples of Cu and Au laser-enhanced exchange plating are shown in Figs. 8(a) and (b). The micrograph for Au shows especially fine grain size in the central region of the laser-enhanced plating. Figure 8(c) shows a similar pattern resulting for Cu/Cu^{++}, where the laser was used to obtain a thermobattery effect.

Mathematical modeling

Some calculations have been made to determine the required temperature and velocity fields of electrolytes for plating in the mass-transport-limited regime. The microstirring which produces the plating enhancement is caused by fluid convection, which is driven by sharp temperature gradients in the electrolyte. Mathematical analysis of this problem requires the solution of coupled three-dimensional time-dependent Navier-Stokes and thermal diffusion equations. As input conditions, the initial temperatures of the fluid and of the surrounding surfaces are required. Mathematical solutions

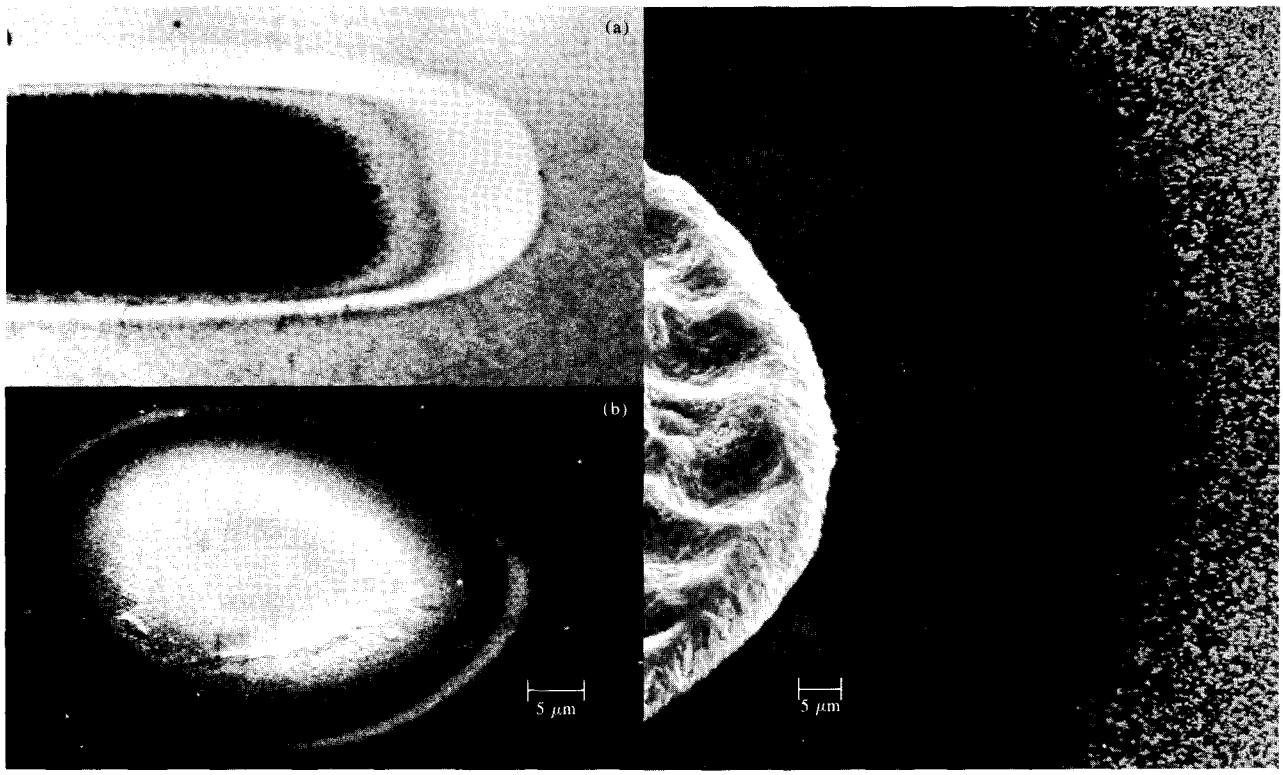

Figure 8 (a) Optical photograph of exchange plating of Cu on 150-nm Ni predeposited film on glass. Etching occurs in the region peripheral to the plated area. Width of plated line is ≈100 μm. (b) SEM micrograph of Au plating on a 150-nm Ti/Cr predeposited layer on glass. (c) SEM micrograph of Cu deposited on Cu with no external electrical circuit. The semicircular deposition pattern of Cu is surrounded by an etched halo region surrounding the plated Cu.

have been obtained for a limited set of input parameters by Langlois [9]. The cathode temperature used in the calculations was based on values obtained from bolometric experiments in which the cathode films used in plating were replaced by a thin-film bolometer [1]. Laser heating of these bolometers results in a time-dependent temperature. For laser beams large in diameter compared to the thermal diffusion spread $\sqrt{kt_0}$, where k is the thermal diffusivity of the substrate and t_0 is the laser pulsewidth, the temperatures were found to increase approximately as $t^{1/2}$ over a large time span, consistent with one-dimensional heat flow for a semi-infinite medium. An example of a voltage–time profile is shown in Fig. 9(a). Independent calibration of the bolometers makes it possible to determine the absolute temperature change occurring during laser irradiation. In the initial experimental work, temperatures were estimated to rise on the order of 50°C in ≈20 ms for incident power densities of $\approx 10^3$ W/cm^2. Additional work to obtain the temperature profile of the laser-irradiated spot and the surrounding region has been described elsewhere [10]. Further work on determining more accurate temperature and fluid-velocity profiles is planned.

Applications and conclusions

Among the many possible uses for laser plating and etching, we have so far concentrated on a few that seem to offer particular promise. These applications require relatively small area and/or randomly located regions of plating or etching. Thus, the technique seems particularly useful as a repair and engineering design-change scheme for microcircuits. In this application, the time-consuming and expensive steps of mask making and photolithography are obviated. As an example of circuit repair, we have demonstrated the bridging of two Cu lines, each ≈12 μm wide and 5 μm thick [4]. The lines were fabricated using standard masking and plating techniques on a glass substrate with a 150-nm predeposited layer of Au to simulate a circuit board. The bridge was made by applying zero overpotential under potentiostatic control and moving a focused Ar laser beam between the two lines. A scanning electron micrograph (SEM) of the circuit after bridging is shown in Fig. 9(b). Subsequent electrical testing of the laser-formed bridge indicated a conductivity comparable to that of the 12-μm plated Cu lines. Other circuits have been repaired using the thermobattery technique. Lines as small as 2 μm wide have

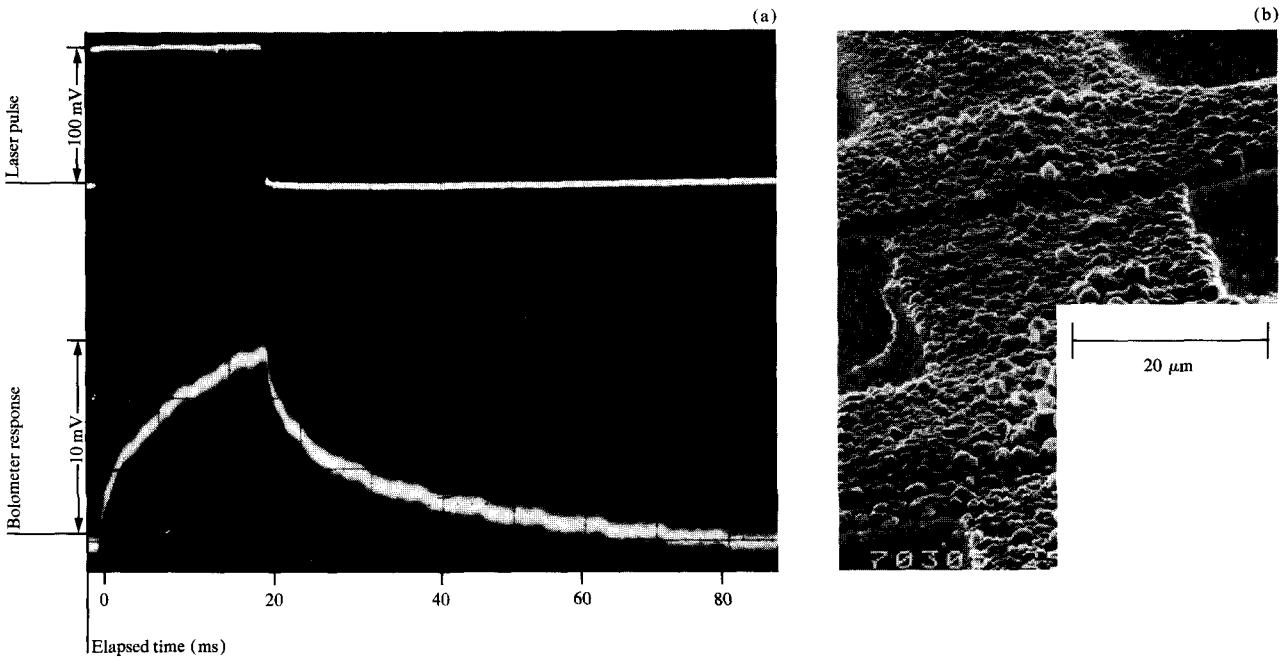

Figure 9 (a) Some voltage–time traces using the set-up of Fig. 1 for pulsed laser illumination incident on a bolometer. The voltage is proportional to temperature. Upper trace, laser pulse; lower trace, bolometer response. (b) SEM micrograph of a laser-enhanced Cu-plated bridge between two previously electroplated Cu lines. The electroplated lines run along the horizontal direction. The predeposited base is Nb (20 nm), Au (150 nm) on a glass substrate.

also recently been fabricated by improving the overall optical resolution of the focusing scheme [4]. Other promising applications include localized plating with precious metals. It is expected that a substantial cost saving can be realized in the electronics industry by localizing the plating of materials such as gold for contact points on connector pins or in crucial contact regions in pin receptacles. Related to this is the possibility of local plating in hard-to-reach regions, such as the inner periphery of small connector holes. Obviously, much work remains to be done both in demonstrating the feasibility of some of these applications and in extending that feasibility to on-line processes. Our initial experiments appear extremely promising and work in all phases of these investigations is continuing.

References and note

1. R. J. von Gutfeld, E. E. Tynan, R. L. Melcher, and S. E. Blum, "Laser Enhanced Electroplating and Maskless Pattern Generation," *Appl. Phys. Lett.* **35,** 651 (1979).
2. R. J. von Gutfeld, E. E. Tynan, and L. T. Romankiw, "Laser Enhanced Electroplating and Etching for Maskless Pattern Generation," Extended Abstract No. 472, *Electrochemical Soc.* 79-2 (1979), 156th Meeting of the Electrochemical Society, Los Angeles, CA.
3. P. Delahay, "Double Layer and Electrode Kinetics," John Wiley & Sons, Inc., New York, 1965, p. 163.
4. J.-Cl. Puippe, R. E. Acosta, and R. J. von Gutfeld, "Investigations of Laser Enhanced Electroplating Mechanisms," *J. Electrochem. Soc.* **128,** 2539 (1981).
5. G. N. Lewis and M. Randall, *Thermodynamics,* McGraw-Hill Book Co., Inc., New York, 1961.
6. J. Newman, *Electrochemical Systems,* Prentice-Hall, Inc., Englewood Cliffs, NJ, 1973.
7. R. J. von Gutfeld and J.-Cl. Puippe, "Laser Enhanced Electroplating and Etching," *Oberfläche-Surface* **22,** 294 (1981).
8. L. H. Kulynych, L. T. Romankiw, and R. J. von Gutfeld, "Laser Enhanced Exchange Plating," *IBM Tech. Disclosure Bull.* **23,** 1262 (1980).
9. For details of the computer program, contact W. E. Langlois, IBM Research Division laboratory, 5600 Cottle Rd., San Jose, CA 95193.
10. L. H. Kulynych, "Investigation of Heat Transfer in Laser Enhanced Electroplating," Bachelor's thesis, Massachusetts Institute of Technology, Cambridge, MA, September 1980.

Received April 6, 1981; revised September 15, 1981

The authors are located at the IBM Thomas J. Watson Research Center, P.O. Box 218, Yorktown Heights, New York 10598.